

Research Article



How to cite: Angew. Chem. Int. Ed. 2025, 64, e202413927 doi.org/10.1002/anie.202413927

Li-ion Batteries

Tuning Reaction Kinetics of Fluorinated Molecules to Construct Robust Solid Electrolyte Interphases on SiO_x **Anode**

Shiming Chen⁺, Zhikang Deng⁺, Jiangxiao Li, Wenguang Zhao, Bowen Nan, Yue Zuo, Jianjun Fang, Yuxiang Huang, Zu-Wei Yin, Feng Pan, and Luyi Yang*

Abstract: Introducing fluorinated electrolyte additives to construct LiF-rich solid-electrolyte interphase (SEI) on Si-based anodes is proven an effective strategy for coping with its massive volume changes during cycling. However, most current research on fluorine-containing additives focuses on their thermodynamics of decomposition, lacking studies on the correlation between the molecular structure of additives and their decomposition kinetics. Herein, two fluorinated ester additives, diethyl fluoromalonate (F1DEM) and diethyl 2,2-difluoromalonate (F2DEM) were designed and synthesized. Through combining a wealth of characterizations and simulations, it is revealed that despite the similar reduction thermodynamics, the favorable reduction kinetics of singlefluorinated F1DEM facilitate a LiF-rich layer during the early stage of SEI formation, contributing to the formation of a more robust SEI on SiO_x anode compared to the difluorinated F2DEM. Consequently, the proposed additive achieves excellent cycling stability (84% capacity retention after 1000 cycles) for 5 Ah 21700 cylindrical batteries under practical testing conditions. By unveiling the role of reaction kinetics, a longoverlooked aspect for the study of electrolyte additives, this work sheds light on how to construct a stable SEI on Si-based anodes.

1. Introduction

To solve the continuous increasing energy demand and environmental concerns looming ahead, developing re-

[*] S. Chen,* Z. Deng,* W. Zhao, B. Nan, Y. Zuo, J. Fang, Y. Huang, F. Pan, L. Yang School of Advanced Materials Peking University Shenzhen Graduate School

Shenzhen 518055, P. R. China E-mail: yangly@pkusz.edu.cn

J. LI

National Synchrotron Radiation Laboratory University of Science and Technology of China Hefei 230029, P. R. China

Z.-W. Yin College of Energy Xiamen University Xiamen, 361005, P. R. China

[+] These authors contributed equally to this work

chargeable lithium-ion batteries (LIBs) with high-energydensity and low cost has been desperately required, stimulating the development of high specific capacity anode materials. [1-3] Representatively, SiO_x (0 < x < 2) material has been deemed as a promising alternative to replace commercially used graphite anode, with the advantages of high theoretical capacity (~1500 mAh g⁻¹), low operation voltage (0.4 V versus Li/Li⁺), environmental friendliness, and abundant resources.^[4] However, it suffers from the vast volume swing (~118%) during lithiation/delithiation process, resulting in particles pulverization, electrode disintegration and continuous growth of solid electrolyte interphase (SEI) and thereby the fast capacity degradation in traditional commercial electrolytes.^[5] In recent years, a number of strategies have been made to optimize SiO_x anode, mainly including structural coating, binder synthesis and electrolyte design.[6-9]

Electrolyte engineering plays a crucial role in tuning the performance of SiO_x anodes. By adjusting the ratio or formulation of lithium salts, solvents, or additives, the cycling performance of the anode under various testing conditions (e.g. elevated temperatures) can be significantly enhanced.[10-13] In particular, using molecular-tailored additives is considered as an economical and efficient approach for improving the electrochemical performance of SiO_x anode. For instance, fluoroethylene carbonate (FEC), a well-established additive for Si-based anodes, was shown to be defluorinated at about 1.0 V (vs. Li/Li⁺) on the surface of Si-based anode, generating lithium fluoride (LiF) and -CHF-OCO₂- type compounds which provides improved mechanical stability interphase and limits the emergence of cracks. [14-16] Moreover, lithium salt additives such as lithium fluorophosphate (LiPO₂F₂, LiDFP) could reduce the decomposition of electrolyte and improve initial coulombic efficiency of Si-based anode.[17] The family of fluorinecontaining electrolyte additives has been extensively studied which have relatively lower lowest unoccupied molecular orbital (LUMO) energy levels generally and contribute to the formation of a stable LiF-rich SEI.

The formation process of the SEI involves the reduction reactions of various electrolyte components (*i.e.*, solvent, lithium salt, and additives). Essentially, the types and amounts of SEI components are determined by the competition between reactions with different reduction thermodynamics and kinetics on the anode surface. In our previous work, we discovered that the stability of the SEI is largely dictated by its early formation process, where additives stabilize the SEI structure by forming a dense and coherent

GDCh

SEI layer that covers the outermost surface of the anode at higher potentials. [18] Therefore, within this relatively short timeframe, the reaction kinetics have a particularly significant impact on the SEI. However, in previous studies, the decomposition kinetics of additives have not received as much attention as their decomposition thermodynamics. Therefore, it is crucial to regulate both the decomposition thermodynamics and kinetics of additives to preferentially form more favorable products during the SEI formation process.

In this work, we design and synthesize diethyl fluoromalonate (F1DEM) and diethyl 2,2-difluoromalonate (F2DEM) as two fluorinated electrolyte additives to explore the relationship between the decomposition kinetics of additives and the SEI formation process (Figure 1a). Compared with the symmetric -CF₂- group, the locally polar -CHF- group not only enables favored Li+ desolvation and more salt anions in solvation configuration, but also shows higher affinity towards the SiO_x surface compared with F2DEM. Additionally, the bond energy of C-F bond in -CHF- group is relatively lower than that in -CF2- group. Exhibiting the superior reduction kinetics to generate LiF over F2DEM, F1DEM enables much faster surface passivation at the early stage of SEI formation. The resultant SEI offers desirable chemo-mechanical properties to accommodate plastic deformation of SiO_x and stabilize the structures of the electrode (Figure 1b). The findings in this study reveal the crucial role of the decomposition kinetics of electrolyte additives in the stability of the SEI.

2. Results and Discussion

Herein, we introduced partially fluorinated -CHF- group and fully fluorinated -CF₂- group to diethyl malonate (DEM), respectively (more details in **Support information**). The corresponding nuclear magnetic resonance (NMR) spectra (Figure S1) confirmed the successful synthesis of F1DEM and F2DEM.[19-21] Density functional theory (DFT) calculation was used to determine the molecular orbital energy levels of ethylene carbonate (EC), ethyl methyl carbonate (EMC), FEC, F1DEM and F2DEM. As shown in Figure 2a, it is clear that the LUMO energies of F1DEM and F2DEM are lower than that of solvents and FEC (as a benchmark), implying the stronger reduction tendency and SEI forming ability of F1DEM and F2DEM on SiO_x anode surface. This could be further confirmed by linear sweep voltammetry (LSV) curves of cells using the baseline electrolyte (1 M LiPF₆ in EC/EMC=3/7 vol %, denoted as BE), 1 vol % F1DEM-containing electrolyte (denoted as BE-F1DEM) and 1 vol % F2DEM-containing electrolyte (denoted as BE-F2DEM) from Figure S2. Interestingly, despite showing a higher LUMO energy, the onset reduction potential of F1DEM (~2.50 V vs Li/Li+) is higher than that of F2DEM (~2.22 V vs Li/Li⁺), demonstrating its preferential decomposition at the anode. To investigate the origin this discrepancy, LSV tests with stepped scanning rates were employed to study the reaction kinetics of additives (Figure 2b and **Figure S3**). [22,23] The shift in peak potential (ΔE_p) of F2DEM with increasing scan rate is larger compared to F1DEM, indicating that its electrochemical reduction is more charge-transfer controlled, which reflects inferior reaction kinetics.

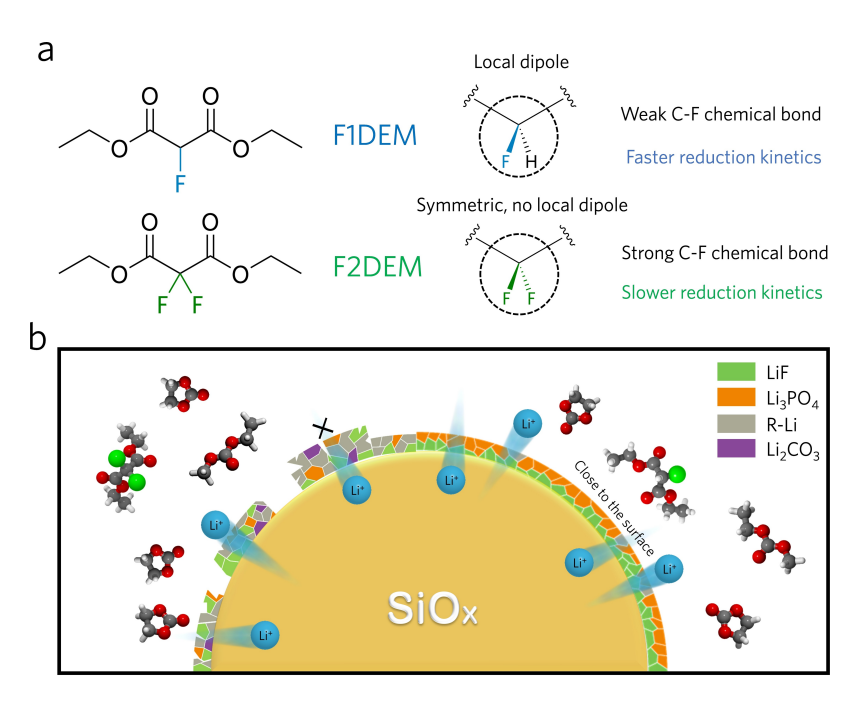


Figure 1. (a) Molecular structures of designed electrolyte additives; (b) Schematic illustration for the F1DEM and F2DEM effect on the formation of the interphase layer on SiO_x anode surface.

5213773, 2025, 1, Downloaded from https://onlinelibrary.wiley.com/doi/10.1002/anie.2024/1927 by University Town Of Shenzhen, Wiley Online Library on [17/1/12025]. See the Terms and Conditions (https://onlinelbrary.wiley.com/terms-and-conditions) on Wiley Online Library for rules of use; OA articles are governed by the applicable Creative Commons. Licensea

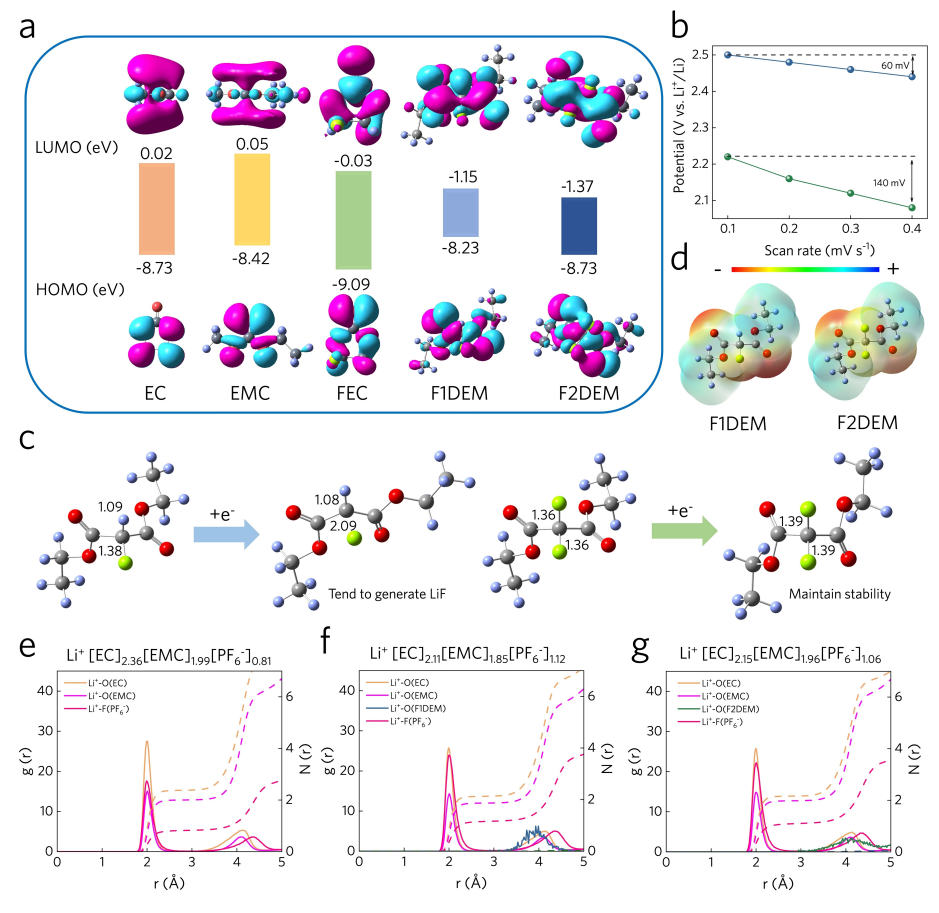


Figure 2. (a) Diagram of calculated HOMO/LUMO energies (eV) of solvents and additives; (b) Relationship between additive decomposition potential and scanning rate; (c) Decomposition path of F1DEM and F2DEM additives (the number in Figure is the length of chemical bond); (d) ESP distribution of F1DEM and F2DEM; Radial distribution functions (RDF) and corresponding 1coordination numbers (N(r)) of BE (e), BE—F1DEM electrolyte (f) and BE—F2DEM electrolyte (g).

In order to elucidate the phenomenon, the Laplacian bond order (LBO) is calculated (Figure S4). It is clear that the bond energy of C-F bond in -CHF- group is relatively lower than that in -CF₂- group, which is attributed to the presence of local polarization that reduces the bond energy of C-F bond. [24] Combing with above LSV curves, the subsequent reduction peak of F1DEM at (~2.20 V vs Li/Li⁺) could attribute to the further decomposition of C-O bonds (Figure S5). Compared with the difluorinated F2DEM, the monofluorinated F1DEM has enol isomers because the C-H bonds are not completely replaced by C-F bonds (Figure S6). Calculations reveal that the C-F bond energy in these isomers is still lower than that in F2DEM, further indicating that the fluorine atoms in F1DEM are more likely to be released. Subsequently, the reduction pathways of additives on the anode side were further investigated by DFT calculation (Figure 2c). After gaining an electron, the C-F bond of F1DEM is dramatically deformed (>1.5 Å) and defluorination reaction occurs, while the C-F bond of F2DEM remains stable, suggesting that F1DEM preferentially undergoes decomposition into SEI.[25] Figure 2d shows the electrostatic potential (ESP) distribution of fluorinated-DEM molecules. For F1DEM, the negative charges were mainly concentrated on C=O group and C-F group, and the F atom in F1DEM was more negative than that in F2DEM, suggesting stronger Li⁺ coordination ability of F1DEM. These results are consistent with the calculated binding energy of Li⁺-fluorinated DEM molecules (**Figure S7** and **Figure S8**). The Li⁺ showed stronger interaction (that is, shorter Li–F distance) with F1DEM molecule (2.06 Å) than F2DEM molecule (2.18 Å). Besides, in heterogeneous reactions, the affinity between the reactants and the substrate also significantly affects the reaction kinetics. Due to the presence of -CH– chemical bonds, F1DEM exhibits a stronger absorption interaction with SiO_x surface (**Figure S9**), which further accelerates its reduction on the anode.

Molecular dynamics (MD) simulations were conducted to investigate the additive influence on Li⁺ solvation sheath and determine the distribution of Li⁺ solvates (Figure 2e-g and **Figure S10**). It is clear that the introduction of F1DEM or F2DEM molecule weakens the interaction between Li⁺ and solvents. The coordination numbers of the first solvation sheath in BE electrolyte with Li⁺ are calculated to be 2.36 (EC), 1.99 (EMC) and 0.81 (PF₆⁻), respectively. After the addition of F1DEM (or F2DEM), the coordination number of EC reduces to 2.11 (or 2.15) but the value of PF₆⁻ increases to 1.12 (or 1.06), indicating enhanced Li⁺-PF₆⁻

5213773, 2025, 1, Downloaded from https://onlinelibrary.wiley.com/doi/10.1002/anie.202413927 by University Town Of Shenzhen, Wiley Online Library on [17/11/2025]. See the Terms and Conditions (https://onlinelbrary.wiley.com/terms-and-conditions) on Wiley Online Library of rules of use; OA articles are governed by the applicable Creative Commons. Licensea

interaction in the electrolyte. Particularly, the Li–O radial distribution functions (RDF) of Li $^+$ -fluorinated DEM molecules demonstrated more F1DEM participating in Li $^+$ solvation than F2DEM by being located in the more inner solvation sheath of Li $^+$ with stronger ion-ion interaction, substantiating the aforementioned DFT results. The above findings are cross-validated by 7 Li NMR nuclear magnetic resonance (NMR) and Raman spectroscopy (**Figure S11** and **Figure S12**). The upfield shifts in 7 Li NMR $^{[26,27]}$ as well as the intensified solvated PF $_6$ $^-$ Raman peak indicate that more contact ion pairs (CIPs) are formed in the presence of additives. The ionic conductivities of various electrolytes were measured, following the trend of BE–F1DEM > BE–F2DEM > BE (**Figure S13**), which is fully consistent with our expectations.

Cyclic voltammograms (CV) of $SiO_x \mid Li$ half cells (**Figure S14**) further demonstrates that F1DEM decomposes preferentially (~2.0 V vs Li/Li⁺) over F2DEM (~1.7 V vs Li/Li⁺) on the SiO_x anode, which agree with the results obtained in Cu||Li cells. The galvanostatic cycling tests of

SiO_x anodes were determined in SiO_x | |Li half-cells. The first-cycle voltage profiles of SiO_x anodes were compared to check the effects of additives on electrochemical behaviors based on real cycling. The same conclusion could be obtained that F1DEM additive is reduced at about 2.0 V earlier than F2DEM at about 1.6 V (Figure S15). As shown in Figure 3a, the BE-F1DEM system exhibits the highest initial Coulombic efficiency (ICE), indicating that the parasitic reactions on the surface of SiO_x anodes have been mitigated during the first lithiation. The capacity of SiO_x anode with BE electrolyte has experienced a dramatic decline, corresponding to a capacity retention of 52.4 % after 100 cycles (Figure 3b). By contrast, both BE-F1DEM and BE-F2DEM electrolytes deliver improved specific capacities of $1338 \,\mathrm{mAh}\,\mathrm{g}^{-1}$ and $1062 \,\mathrm{mAh}\,\mathrm{g}^{-1}$ after 100 cycles, corresponding to the higher capacity retention of 92.8 % and 74.1% respectively. Especially, BE-F1DEM exhibits the highest cycling stability (~80 % capacity retention after 200 cycles) during the long-term test. For the cell using BE, the increasing overpotentials (Figure S16) and electrochemical

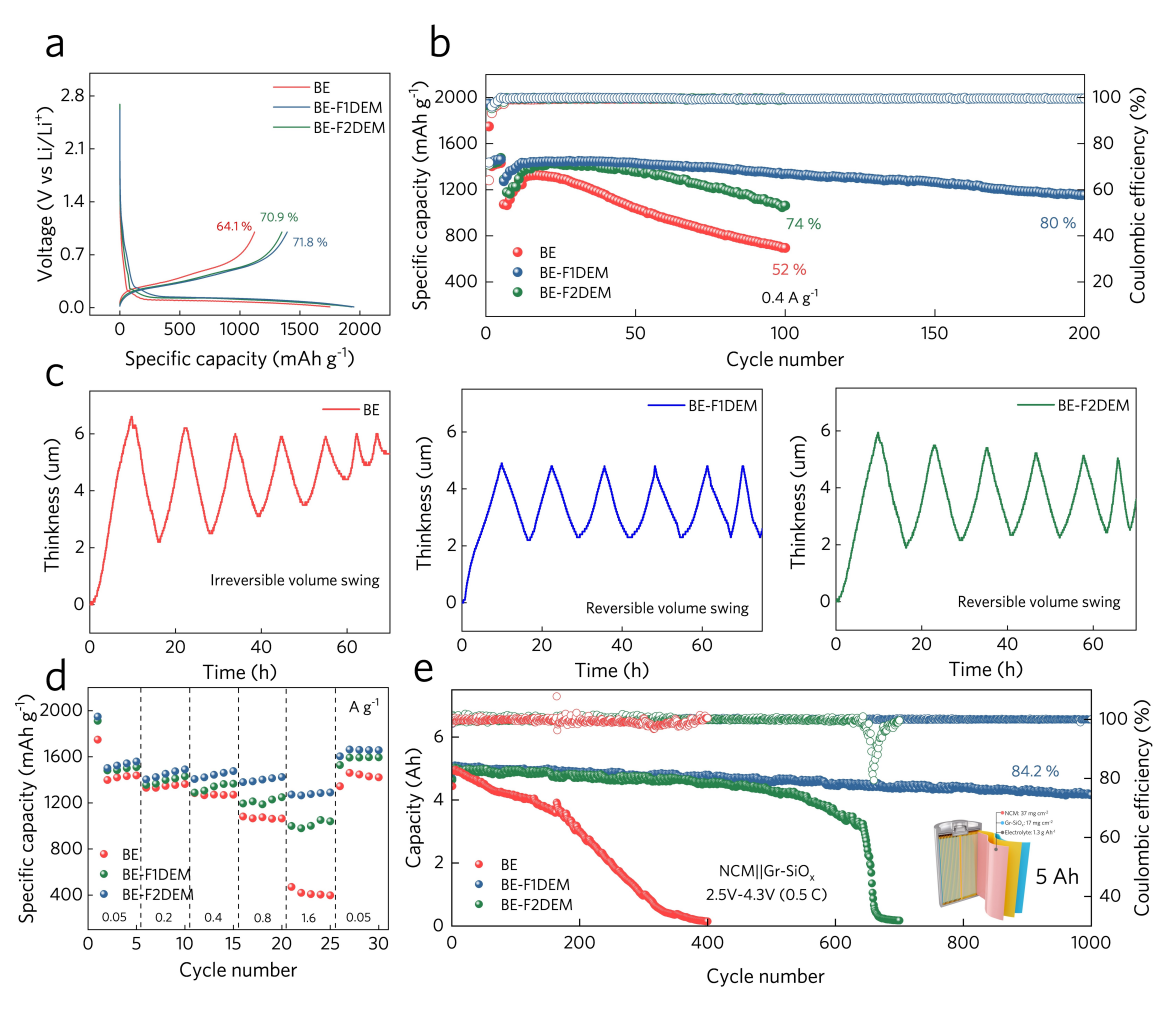


Figure 3. (a) Voltage profiles of SiO_x anodes with various electrolytes for the 1st cycle; (b) Galvanostatic cycling performance and Coulombic efficiency of SiO_x | Li cells with various electrolytes at a current density of 0.05 A g⁻¹ for the first 5 cycles and 0.4 A g⁻¹ for the subsequent cycles; (c) in situ expansion ratio measurements of NCM | $|SiO_x|$ cells with various electrolytes at a current density of 0.1 C for the first 5 cycles and 0.2 C for the subsequent cycles; (d) Rate performance of SiO_x | Li cells with various electrolytes; (e) Galvanostatic cycling performance and Coulombic efficiency of 21700 cylindrical cells at a rate of 0.5 C using various electrolytes.



impedances of SEI (R_{SEI} , Figure S17) during the cycling can be attributed to the unrestricted growth of SEIs and the thickening of electrodes.^[5] To verify this speculation, volume change of SiO_x electrodes was in situ measured by a Swagelok-type cell connected to a thickness detecting instrument (Figure 3c and Figure S18). The swelling ratio curves indicate that the cell with BE exhibited a consistent trend of increasing irreversible volume changes, which arises from the uneven growth of SEI. In contrast, SiO_x electrodes cycled in BE-F1DEM and BE-F2DEM demonstrated better reversibility in expansion and contraction, indicating that the fluorine-containing additives help to form more resilient SEIs. In particular, a lower volume variation ratio was achieved in BE-F1DEM compared with that measured in BE-F2DEM, suggesting the SEI initially constructed in BE-F1DEM was more compact, reducing the overall expansion rate of the electrode. Similar results can be observed from the cross-sectional SEM images after 20 cycles (Figure S19), where the electrode cycled in BE-F1DEM exhibits the lowest thickness variation. It should be noted that, even under a high specific current of 0.8 A g⁻¹, BE-F1DEM still facilitates good cycle stability with 88.8 % capacity retention (Figure S20) after 100 cycles, suggesting that the decomposition of F1DEM contributes to the construction of a robust SEI to tolerate fast SiO_x expansion and contraction.

Apart from cycle stability, the SiO_x anode with BE-F1DEM electrolyte also presents the best rate performance with a specific capacity of 1265 mAh g⁻¹ even at a large current of 1.6 Ag⁻¹ (Figure 3d and Figure S21, which is significantly higher than that of BE–F2DEM (1025 mAh g⁻¹) and BE (459 mAh g⁻¹). After increasing the current to $3.2 \,\mathrm{Ag^{-1}}$, the SiO_x anode with BE-F1DEM delivers a specific capacity of 641 mAh g⁻¹ (Figure S22). The energy barrier of Li^+ penetrating through SEI (E_a) were calculated by the Arrhenius equation based on the electrochemical impedance spectroscopy (EIS) at different temperatures (Figure S23). The value of E_a for BE, BE-F1DEM, and BE-F2DEM electrolyte is 62.07, 41.39, and 52.83 kJ mol⁻¹, respectively, suggesting that an SEI more conducive to Li⁺ is formed in BE-F1DEM electrolyte. The galvanostatic intermittent titration technique (GITT) measurement is used to evaluate the Li^+ diffusion coefficients (D_{Li^+}) , which reflects the diffusion rate of Li+ at the interphase (Figure S24). The higher $D_{\text{Li}+}$ obtained in the BE-F1DEM system indicates the accelerated interphasial migration of Li⁺. Therefore, it can be concluded that F1DEM enables an SEI with faster Li⁺ conducting channels, leading to the enhanced rate performance. For comparison, 1 vol % commercially used fluoroethylene carbonate (FEC) additivecontaining electrolyte (denoted as BE-FEC) was also tested (Figure S25). In terms of ICE, rate capability and cycle life, BE-FEC exhibits inferior performance compared with both BE-F1DEM and BE-F2DEM.

To validate the application potential of proposed additives in full cells, we assembled and tested $\text{LiNi}_{0.83}\text{Co}_{0.12}\text{Mn}_{0.05}\text{O}_2$ (NCM)||SiO_x full cells. It is found that the addition of F1DEM significantly enhanced the cycling performance of the full cells, with a capacity

retention rate of 90.8% after 100 cycles (Figure S26). Besides, the full cell with BE-F1DEM delivers the best rate performance with a specific capacity of ~90 mAh g⁻¹ at 4 C (Figure S27). To further demonstrate the advantage of partially fluorinated additive, proof-of-concept NCM|| graphite (Gr)-SiO_x cylindrical cells (~5 Ah) were assembled and tested under practical conditions (Figure 3e and Figure \$28). The capacity ratio of anode to cathode is 1.08 and the cylindrical cells were tested under lean electrolytes (1.3 g Ah⁻¹). From the dQ/dV curves of cells (**Figure S29**), the intensity of Peak 1 and Peak 2 is reduced in BE and BE-F2DEM electrolytes, indicating the loss of active materials.^[29,30] In comparison, BE–F1DEM electrolyte delivered high capacity retention of 84.2 % and average CE of 99.97% after 1000 cycles with no obvious loss of negative active materials and Li. Despite showing good capacity retention initially, the capacity of the cell with BE-F2DEM showed serious deterioration during subsequent cycling (~600 cycles), indicating the F2DEM-derived SEI is less stable compared with the F1DEM-derived one.

In situ FTIR was performed to reveal the interfacial evolution of various electrolytes during SEI formation (Figure 4a-c and Figure S30). Upon discharging SiO_x anode from OCV to 0.01 V, significant changes were observed in the BE electrolyte, indicating of the excessive decomposition of electrolyte solvents. The peak intensity of EC $(\sim 1800 \text{ cm}^{-1})$, Li⁺-EC $(\sim 1770 \text{ cm}^{-1})$, EMC $(\sim 1750 \text{ cm}^{-1})$ and Li⁺-EMC (~1715 cm⁻¹) exhibit obvious attenuation, and the increased peak intensity of dehydrogenated EC (de-H EC, one hydrogen removed, ~1827 cm⁻¹), dehydrogenated EMC (de-H EMC, one hydrogen removed, ~1761 cm⁻¹, $\sim\!1754~cm^{-1}$ and $\sim\!1738~cm^{-1})$ is found. ^[31] By contrast, the corresponding peaks of above-mentioned solvent decomposition and side reaction product are dramatically inhibited at the presence of F1DEM and F2DEM additives. It is worth noting that the stronger inhibiting effect is exhibited by F1DEM than F2DEM, which could be attributed to the prior decomposition of F1DEM forms a robust passivation interphase, suppressing unlimited decompositions of electrolyte.

Next, in situ EIS of SiOx anodes at the first cycle was carried out to reveal the forming process of SEI in various electrolytes (Figure 4d-f). The resistance of SEI (R_{SEI}) and Li^+ charge transfer (R_{ct}) rapidly stabilized and remained stable during cycling in BE-F1DEM electrolyte, suggesting F1DEM induced an SEI layer with lower interfacial resistance and excellent stability which effectively prevents the interfacial side reactions. In comparison, the impedance measured in BE and BE-F2DEM gradually increased, indicating the formation of unstable interphases which are vulnerable to volume swing and electrolyte. [32] In addition, the composition evolution of SEI during its formation process in various electrolytes was recorded by X-ray photoelectron spectroscopy (XPS) under different potentials (Figure 4g-i). Due to the absence of fluorinated additives, negligible LiF generation in BE between 2.2 and 1.6 V. In contrast, in the presence of F1DEM, the LiF signal was detectable as early as 2.2 V and increased rapidly, confirming the generation of a LiF-rich layer in the initial stages of

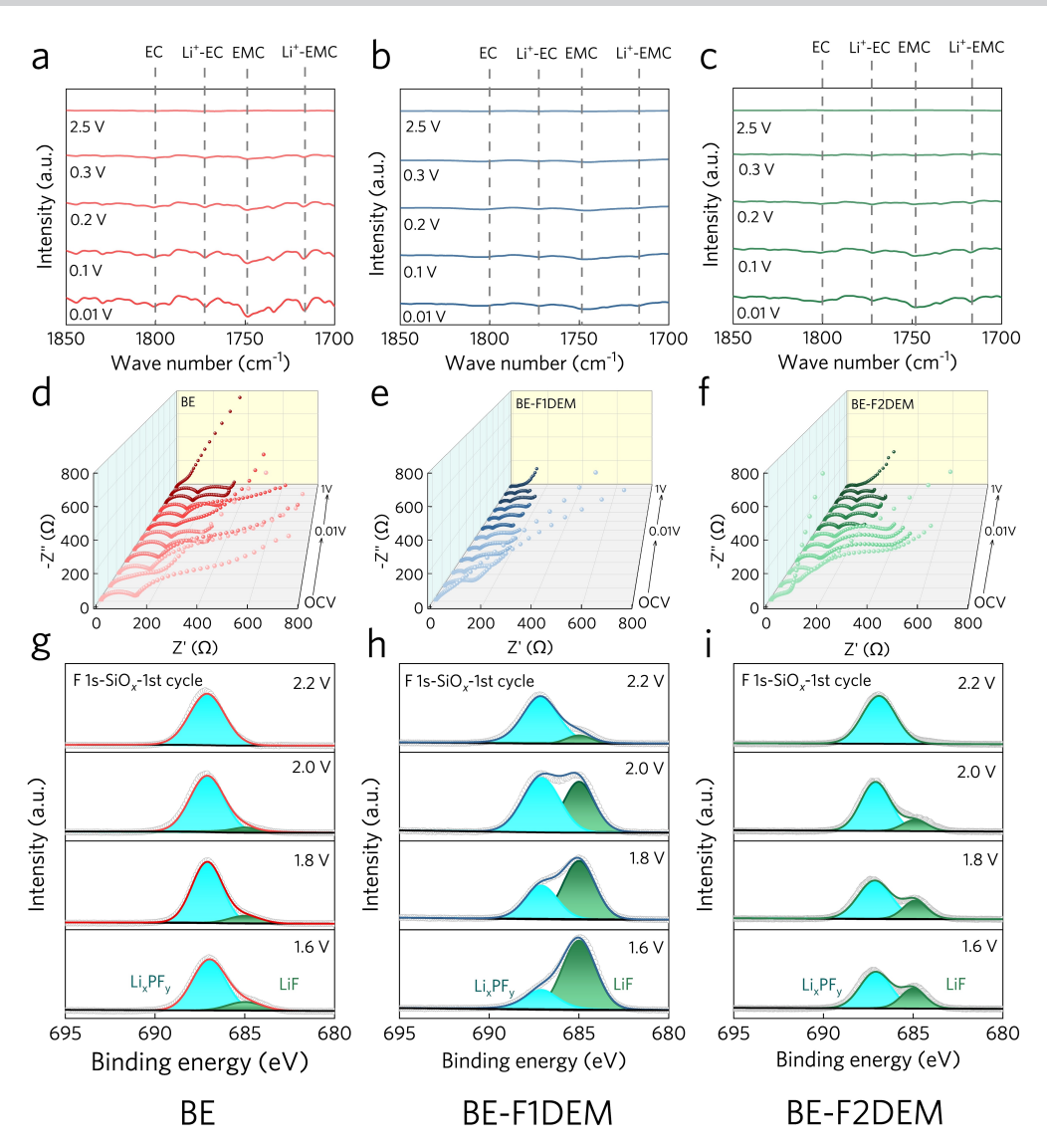


Figure 4. In situ FTIR difference spectra (C=O stretching region) on SiO_x anode surface during galvanostatic discharging to 0.01 V with BE (a), BE-F1DEM (b) and BE-F2DEM (c) electrolytes; In situ EIS of SiO_x | |Li cells with BE (d), BE-F1DEM (e) and BE-F2DEM (f) at the first cycle; F1s X-ray photoelectron spectroscopy (XPS) spectra of SiO_x anodes with BE (g), BE-F1DEM (h) and BE-F2DEM (i) at 1st discharge under different potentials.

SEI formation. For the BE–F2DEM system, the emergence of the LiF signal occurred later and its growth was slower compared to the BE–F1DEM system. Both EIS and XPS results confirmed that the faster decomposition of F1DEM facilitates preferential formation of LiF at relatively high potentials (>1.6 V vs Li/Li $^+$), which could better passivate the SiO $_{\rm x}$ anode surface for subsequent reactions.

The chemical compositions of SEI layers were investigated by XPS to reveal the underlying reason for improved stability and reduced impedance of the SEI formed in BE-F1DEM (Figure 5a, Figure 5b, Figure S30-S35). Considering the similar structure of F1DEM and F2DEM, the SEIs formed in both electrolytes show very similar compositions after 5 cycles, with abundant inorganic species, especially LiF (mainly originated from the decomposition of additives). It is worth noting that the SiO_x anode exhibits strong -OCO₂Li signals cycled in BE, which derives from

reduction decomposition of carbonate solvents. A small portion of the LiF component detached from the SEI during cycling due to significant volume swings and was replaced by other species. Combining C1s (Figure 5a and Figure S33), F1s (Figure 5b and Figure S34) and Li 1s (Figure S35) spectra after 100 cycles, both BE-F1DEM and BE-F2DEM samples show high intensity of LiF in the SEI layer, with Li₃PO₄ and Li₂CO₃, Li_xPF_v observed respectively. To corroborate, soft X-ray absorption spectroscopy (sXAS) data of SiO_x anodes with total electron yield TEY mode (<5 nm) are collected to resolve the SEI components. As shown in Figure 5c, there are more Li₂CO₃ (~534 eV) and lithium carboxylate (~544 eV) species generated on the SiO_x surface in BE and BE-F2DEM electrolytes. [33] The F K-edge spectra (Figure 5d) showed four clearly distinguishable peaks centered at ~691.6 eV (P-F), ~692.7 eV (LiF), 696.6 eV (P-F) and ~702 eV (LiF). [34,35] After 100 cycles, the clear peak of 15213773, 2025, 1, Downloaded from https://onlinelibrary.wiley.com/doi/10.1002/anie.2024/1927 by University Town Of Shenzhen, Wiley Online Library on [17/11/2025]. See the Terms and Conditions (https://onlinelibrary.wiley.com/terms-and-conditions) on Wiley Online Library of rules of use; OA articles are governed by the applicable Creative Commons. License

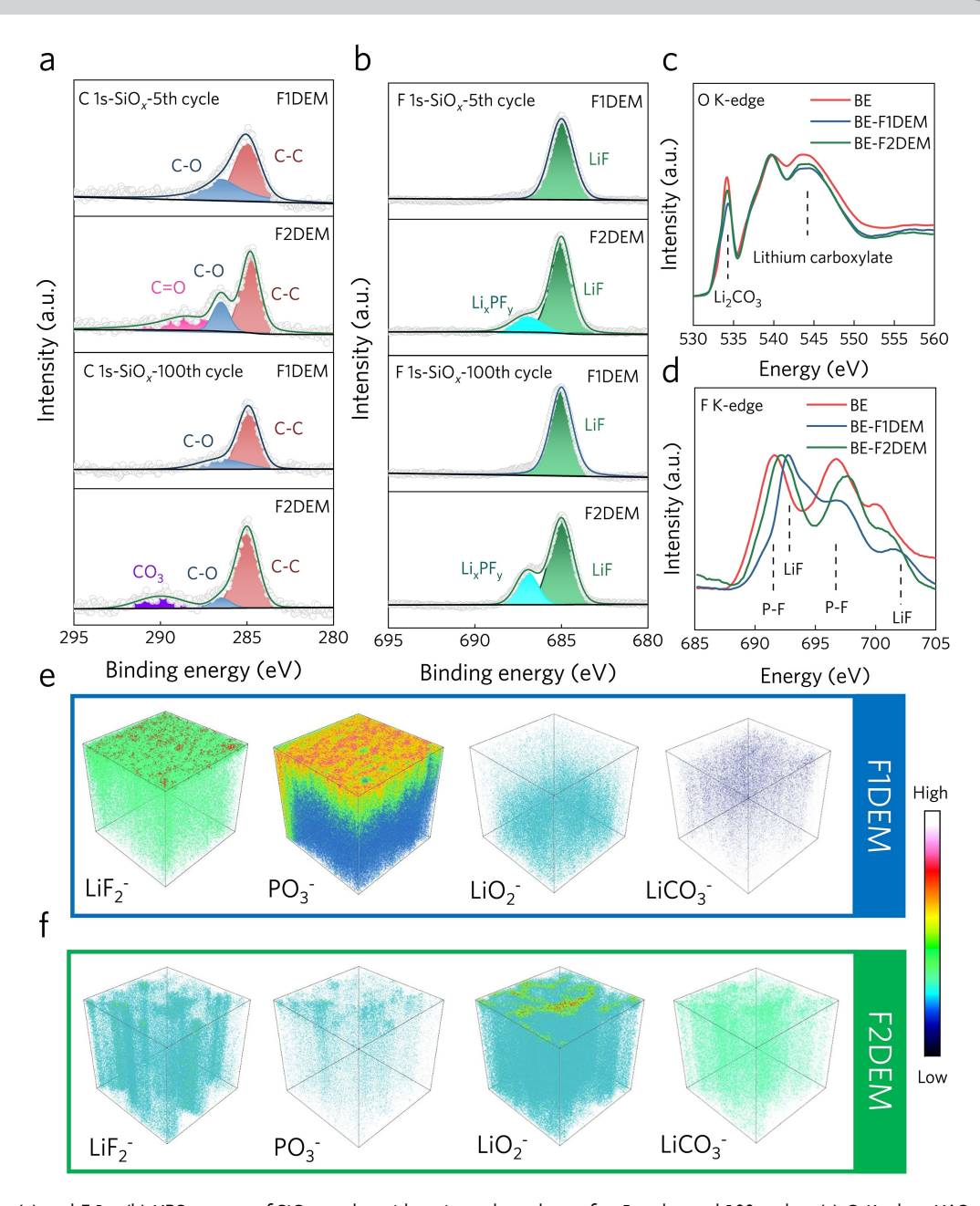


Figure 5. C 1 s (a) and F 1 s (b) XPS spectra of SiO_x anodes with various electrolytes after 5 cycles and 100 cycles; (c) O K-edge sXAS results of SiO_x anodes with various electrolytes after 100 cycles; (d) F K-edge sXAS results of SiO_x anodes with various electrolytes after 100 cycles. (e) TOF-SIMS three-dimensional distributions on SiO_x anodes in full cells with BE-F1DEM (a) and BE-F2DEM (b) electrolytes after 100 cycles (the higher color saturation representing the higher content).

LiF could be seen in BE–F1DEM system, while more P–F signals were observed for BE–F2DEM, further corroborating the XPS results. As previously mentioned, the introduction of F1DEM contributes to the formation of more CIPs, thus, a SEI dominated by anion-derived decomposition products (LiF and Li₃PO₄) is formed, which favors the Li⁺ transfer through the SEI. [36-38]. In addition, its favored decomposition kinetics result in a robust SEI with a dense Li-rich inner layer at relatively high potentials. With a better passivating interphase, excess carbonate decomposition can be effectively suppressed.

To explore the spatial distribution of different chemical components within SEI, time of flight secondary-ion mass spectroscopy (TOF-SIMS) measurements were carried out (Figure 5e, Figure 5f and **Figure S36**). The intense LiF_2^- and PO_3^- signals uniformly detected on the SiO_x surface verifies that the F1DEM-induced SEI is mainly composed of inorganic constituents generated from the decomposition of additives and lithium salts, well agreeing with the XPS results. The species of LiO_2^- and LiCO_3^- correspond to the reduction products of EC and EMC solvents, such as lithium alkyl esters and Li_2CO_3 . Compared with F1DEM, an SEI with larger amount of solvent-derived components was

15213773, 2025, 1, Downloaded from https://onlinelibrary.wiley.com/doi/10.1002/anie.2024/1927 by University Town Of Shenzhen, Wiley Online Library on [17/11/2025]. See the Terms and Conditions (https://onlinelibrary.wiley.com/terms-and-conditions) on Wiley Online Library of rules of use; OA articles are governed by the applicable Creative Commons. License

formed in BE–F2DEM electrolyte, indicating the insufficiency of inorganic passivating species (*i.e.* LiF) generated during the early stages of SEI formation prevent it from effectively passivating the SiO_x surface. Moreover, as a SEI component with high lithium-ion conductivity, the content of Li₃PO₄ in the F1DEM-derived SEI, especially on the outermost surface, is much higher than that derived from F2DEM. This difference suggests that the former could better tolerate the repeated volume swings, hence mechanically fragile components like lithium phosphate can be better retained in the SEI. Exhibiting a LiF-rich inner layer and a Li₃PO₄-rich outer layer, the hierarchically structured SEI formed in BE–F1DEM not only promotes the interphasial stability for long-term cycling, but also facilitate fast interphasial Li⁺ conduction for high-rate operation.

The microstructure of SEI formed in different electrolytes was further examined by cryo-transmission electron microscopy (cryo-TEM). A fractured and uneven SEI layer is evident on the SiO_x anode cycled in BE electrolyte after 100 cycles (Figure 6a). In comparison, the SEI formed in BE–F1DEM electrolyte remain intact, protected by a uni-

form and thin SEI, confirming the suppressed electrolyte decomposition and the intact structure of SiO_x anode after multiple cycles at the present of F1DEM (Figure 6b), a relatively thicker SEI was generated in BE–F2DEM, suggesting the existence of excess electrolyte decomposition (Figure 6c).

To evaluate the mechanical properties of SEI formed on SiO_x surface in BE, BE–F1DEM and BE–F2DEM electrolytes, atomic force microscopy (AFM) measurements were performed. The SiO_x particle cycled in BE–F1DEM exhibits a more uniform and smoother surface morphology compared to that cycled in BE and BE–F2DEM electrolytes (**Figure S37**), which well agrees with the cryo-TEM results. More importantly, the corresponding Derjaguin-Müller-Toporov (DMT) modulus of BE–F1DEM electrolyte derived SEI exhibits a high average value of 3.83 GPa, much higher than that of BE (0.96 GPa) and BE–F2DEM (2.73 GPa), which could be due to the higher content of inorganic species (Figure 6d–f). Generally, an SEI with high Young's modulus could better restrict the volume expansion and maintain the integrity of SiO_x electrodes. For a more

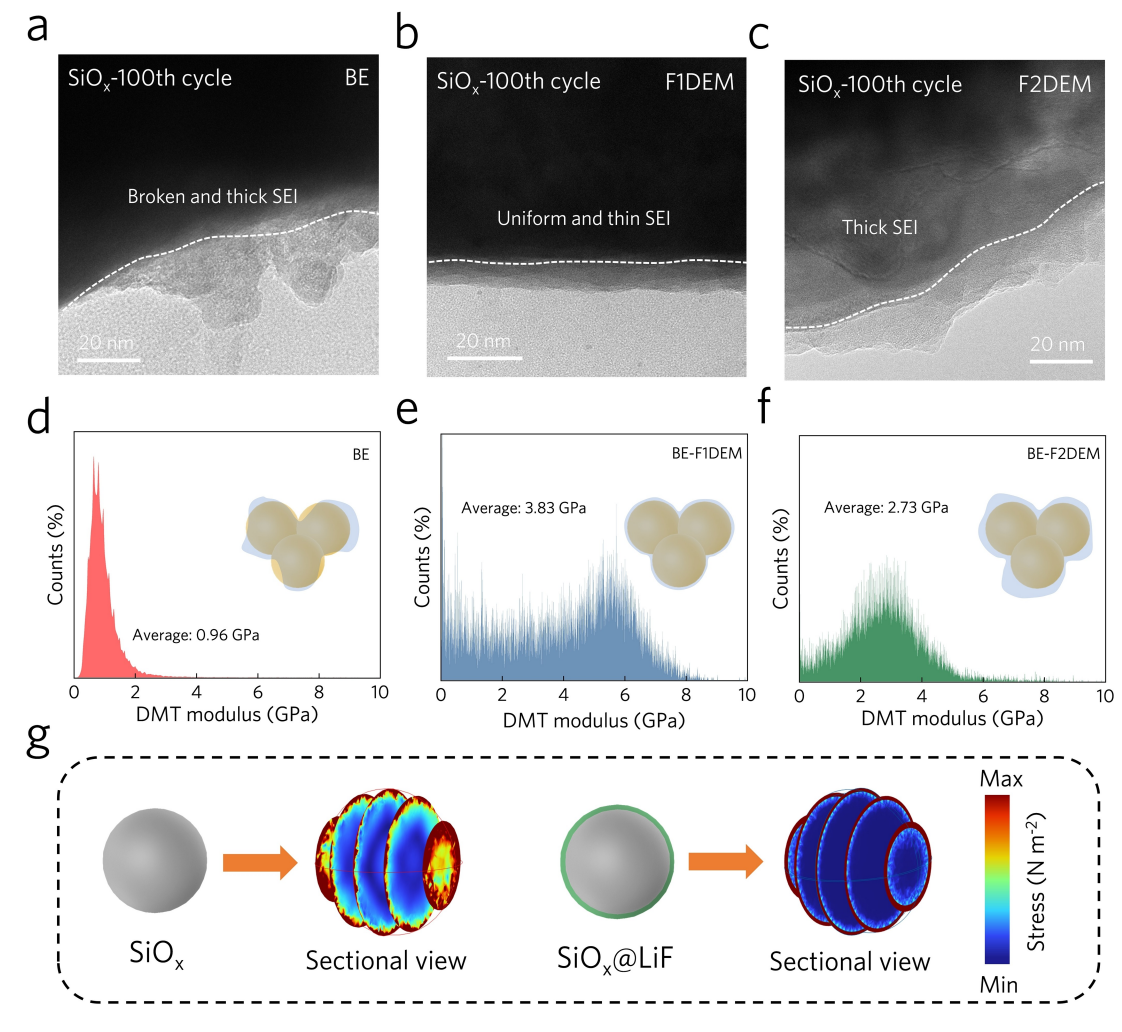


Figure 6. Cryo-TEM images of SiO_x anodes with BE (a), BE-F1DEM (b) and BE-F2DEM (c) electrolytes at delithiated state after 100 cycles; DMT modulus distribution of SEI on the SiO_x anodes after 100 cycles with BE (d), BE-F1DEM (e) and BE-F2DEM (f) electrolytes; (g) Cross-sectional view of the stress distribution for pristine SiO_x particle and SiO_x particle coating with LiF.

vivid demonstration, simulation based on finite element method (FEM) was applied to describe the stress mitigation effect of stable SEI layer. As displayed in Figure 6g, the bare SiO_x particle undergoes sharp stress accumulation from the outer surface to the inner bulk. Conversely, the stress evolution of the SiO_x particle exhibits a gradual trend when subject to the interfacial coating of a LiF layer, with the primary stress concentrated within the LiF layer. The different stress distribution behaviors of both particles are attributed to the LiF interface with high Young's modulus and low adhesion. [8,40] The above findings further demonstrate that the incorporation of F1DEM additive helps to form a mechanically durable SEI film, which effectively mitigates the volume change and minimizes stress concentration during repeated cycling.

3. Conclusions

In summary, we prepared two additives with different fluorine content (F1DEM and F2DEM) to improve the interphase stability of silicon-based anodes. A series of characterizations revealed that, despite having a lower fluorine content, F1DEM with partially fluorinated –CHF–groups exhibits better decomposition kinetics compared to F2DEM. Consequently, F1DEM can quickly form a LiF-rich passivation layer on the anode surface during the initial stages of SEI formation (Scheme 1). This layer effectively

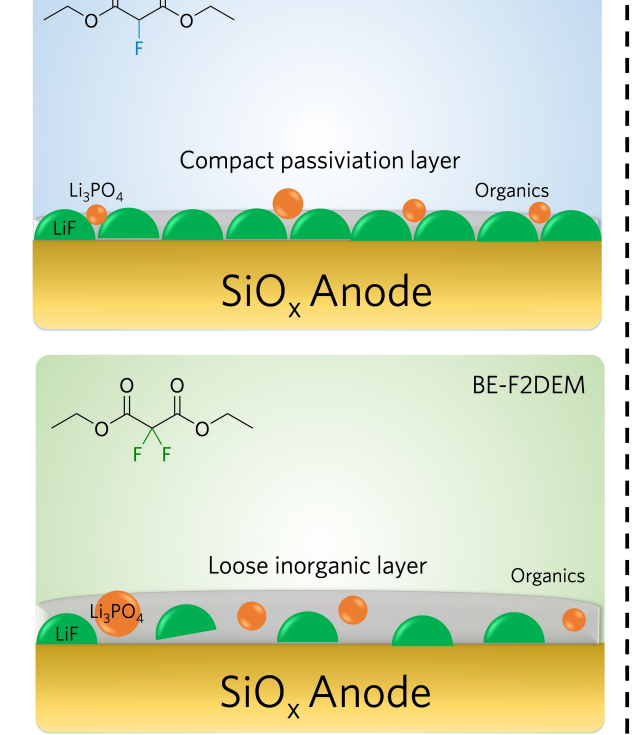
suppresses side reactions and better accommodates volume changes, thus stabilizing the interfacial structure and composition. In contrast, while F2DEM can also form a significant amount of LiF, its poorer decomposition kinetics prevent it from quickly passivating the anode surface during the initial SEI formation stages. This results in a thicker and mechanically weaker SEI. By revealing the impact of fluorinated additive decomposition kinetics on SEI formation and the electrochemical performance of silicon-based anodes, this work provides new insights for constructing stable interfaces in high-energy-density batteries.

Acknowledgements

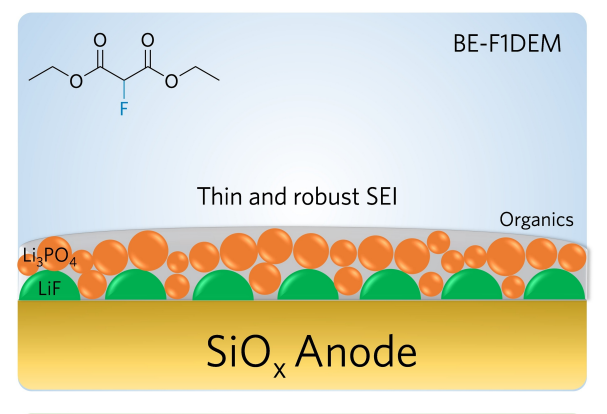
This work was financially supported by National Natural Science Foundation of China (No. 52303263) and Shenzhen Science and Technology Research Grant (No. ZDSYS201707281026184). The authors thank the support from the XMCD beamline (BL12B) in the National Synchrotron Radiation Laboratory (NSRL) and Shanghai Synchrotron Radiation Facility (SSRF) (beamline 02B02).

Early stage of SEI formation

BE-F1DEM



Ultimately formed SEI





Scheme 1. Schematic illustration of the impact of additives with different decomposition kinetics on the initial growth and final morphology of SEI.





Conflict of Interest

The authors declare that they have no known competing financial interests or personal relationships that could have appeared to influence the work reported in this paper.

Data Availability Statement

The data that support the findings of this study are available from the corresponding author upon reasonable request.

Keywords: fluorination extent \cdot SiO_x anode \cdot solid electrolyte interphase \cdot reduction thermodynamics and kinetics

- [1] J. B. Goodenough, Y. Kim, Chem. Mater. 2010, 22, 587.
- [2] Q. Shi, J. Zhou, S. Ullah, X. Yang, K. Tokarska, B. Trzebicka, H. Q. Ta, M. H. Rümmeli, Energy Storage Mater. 2021, 34, 735.
- [3] Z. Chen, A. Soltani, Y. Chen, Q. Zhang, A. Davoodi, S. Hosseinpour, W. Peukert, W. Liu, Adv. Energy Mater. 2022, 12, 2200924.
- [4] Z. Liu, Q. Yu, Y. Zhao, R. He, M. Xu, S. Feng, S. Li, L. Zhou, L. Mai, Chem. Soc. Rev. 2019, 48, 285.
- [5] G. Qian, Y. Li, H. Chen, L. Xie, T. Liu, N. Yang, Y. Song, C. Lin, J. Cheng, N. Nakashima, M. Zhang, Z. Li, W. Zhao, X. Yang, H. Lin, X. Lu, L. Yang, H. Li, K. Amine, L. Chen, F. Pan, Nat. Commun. 2023, 14, 6048.
- [6] F. Wang, J. Mao, Y. Zhao, Adv. Mater. 2023, 35, 2307908.
- [7] T. Zhu, H. Sternlicht, Y. Ha, C. Fang, D. Liu, B. H. Savitzky, X. Zhao, Y. Lu, Y. Fu, C. Ophus, C. Zhu, W. Yang, A. M. Minor, G. Liu, *Nat. Energy* 2023, 8, 129.
- [8] J. Chen, X. Fan, Q. Li, H. Yang, M. R. Khoshi, Y. Xu, S. Hwang, L. Chen, X. Ji, C. Yang, H. He, C. Wang, E. Garfunkel, D. Su, O. Borodin, C. Wang, Nat. Energy 2020, 5, 386
- [9] X. Zhuang, S. Zhang, Z. Cui, B. Xie, T. Gong, X. Zhang, J. Li, R. Wu, S. Wang, L. Qiao, T. Liu, S. Dong, G. Xu, L. Huang, G. Cui, Angew. Chem. Int. Ed. 2024, 63, e202315710.
- [10] H. Jia, P. Gao, L. Zou, K. S. Han, M. H. Engelhard, Y. He, X. Zhang, W. Zhao, R. Yi, H. Wang, C. Wang, X. Li, J. G. Zhang, Chem. Mater. 2020, 32, 8956.
- [11] K. Xu, Chem. Rev. 2014, 114, 11503.
- [12] O. Borodin, X. Ren, J. Vatamanu, A. Von Wald Cresce, J. Knap, K. Xu, Acc. Chem. Res. 2017, 50, 2886.
- [13] T. Dong, S. Zhang, Z. Ren, L. Huang, G. Xu, T. Liu, S. Wang, G. Cui, Adv. Sci. 2024, 11, 2305753.
- [14] V. Etacheri, O. Haik, Y. Goffer, G. A. Roberts, I. C. Stefan, R. Fasching, D. Aurbach, *Langmuir* 2012, 28, 965.
- [15] Y. Jin, N. J. H. Kneusels, L. E. Marbella, E. Castillo-Martínez, P. C. M. M. Magusin, R. S. Weatherup, E. Jónsson, T. Liu, S. Paul, C. P. Grey, J. Am. Chem. Soc. 2018, 140, 9854.
- [16] C. Xu, F. Lindgren, B. Philippe, M. Gorgoi, F. Björefors, K. Edström, T. Gustafsson, *Chem. Mater.* 2015, 27, 2591.
- [17] C. Li, W. Zhu, B. Lao, X. Huang, H. Yin, Z. Yang, H. Wang, D. Chen, Y. Xu, *ChemElectroChem* **2020**, *7*, 3743.

- [18] Y. Ji, J. Qiu, W. Zhao, T. Liu, Z. Dong, K. Yang, G. Zheng, G. Qian, M. Yang, Q. Chen, K. Amine, F. Pan, L. Yang, *Chem* 2023, 9, 2943.
- [19] F. Jiang, Y. Zhao, J. Hu, Org. Chem. Front. 2014, 1, 625.
- [20] T. Umemoto, S. Fukami, G. Tomizawa, K. Harasawa, K. Kawada, K. Tomital, J. Am. Chem. Soc. 1990, 112, 8563.
- [21] Y. Yang, G. B. Hammond, T. Umemoto, Angew. Chem. Int. Ed. 2022, 61, e202211688.
- [22] R. S. Nicholson, Anal. Chem. 1965, 37, 1351.
- [23] L. H. Han, J. Y. Guo, M. M. Cui, *J. Electrochem. Soc.* **2024**, *30*, 230321.
- [24] T. Lu, F. Chen, J. Phys. Chem. A 2013, 117, 3100.
- [25] H. Amii, K. Uneyama, Chem. Rev. 2009, 109, 2119.
- [26] Q. Sun, Z. Cao, Z. Ma, J. Zhang, W. Wahyudi, T. Cai, H. Cheng, Q. Li, H. Kim, E. Xie, L. Cavallo, Y. K. Sun, J. Ming, ACS Materials Lett. 2022, 4, 2233.
- [27] Y. Chen, Z. Yu, P. Rudnicki, H. Gong, Z. Huang, S. C. Kim, J. C. Lai, X. Kong, J. Qin, Y. Cui, Z. Bao, J. Am. Chem. Soc. 2021, 143, 18703.
- [28] Z. Yu, P. E. Rudnicki, Z. Zhang, Z. Huang, H. Celik, S. T. Oyakhire, Y. Chen, X. Kong, S. C. Kim, X. Xiao, H. Wang, Y. Zheng, G. A. Kamat, M. S. Kim, S. F. Bent, J. Qin, Y. Cui, Z. Bao, *Nat. Energy* 2022, 7, 94.
- [29] A. J. Smith, J. C. Burns, J. R. Dahn, Electrochem. Solid-State Lett. 2011, 14, 12.
- [30] S. Li, S. Tsutsumi, S. Shironita, M. Umeda, *Electrochemistry* 2022, 90, 2.
- [31] Y. Zhang, Y. Katayama, R. Tatara, L. Giordano, Y. Yu, D. Fraggedakis, J. G. Sun, F. Maglia, R. Jung, M. Z. Bazant, Y. Shao-Horn, *Energy Environ. Sci.* 2020, 13, 183.
- [32] C. Deng, H. Wang, S. Wang, J. Mater. Chem. A 2021, 9, 15734.
- [33] F. Wu, Y. Dong, Y. Su, C. Wei, T. Chen, W. Yan, S. Ma, L. Ma, B. Wang, L. Chen, Q. Huang, D. Cao, Y. Lu, M. Wang, L. Wang, G. Tan, J. Wang, N. Li, Small 2023, 2301301, 1.
- [34] J. E. N. Swallow, M. W. Fraser, N. J. H. Kneusels, J. F. Charlton, C. G. Sole, C. M. E. Phelan, E. Björklund, P. Bencok, C. Escudero, V. Pérez-Dieste, C. P. Grey, R. J. Nicholls, R. S. Weatherup, *Nat. Commun.* 2022, 13, 6070.
- [35] F. Wu, Y. Dong, Y. Su, C. Wei, T. Chen, W. Yan, S. Ma, L. Ma, B. Wang, L. Chen, Q. Huang, D. Cao, Y. Lu, M. Wang, L. Wang, G. Tan, J. Wang, N. Li, Small 2023, 19, 2301301.
- [36] S. S. Zhang, X. Fan, C. Wang, ChemElectroChem 2019, 6, 1536.
- [37] J. Dutta, S. Ghosh, K. K. Garlapati, S. K. Martha, J. Power Sources 2023, 587, 233717.
- [38] R. Wu, X. Du, T. Liu, X. Zhuang, P. Guan, B. Zhang, S. Zhang, C. Gao, G. Xu, X. Zhou, G. Cui, Adv. Energy Mater. 2024, 14, 2302899.
- [39] X. Yang, Y. Huang, J. Li, W. Huang, W. Yang, C. Wu, S. Tang, F. Ren, Z. Gong, N. Zhou, Y. Yang, *Energy Mater.* 2023, 3, 200020.
- [40] T. Yu, T. Zhao, N. Zhang, T. Xue, Y. Chen, Y. Ye, F. Wu, R. Chen, Nano Lett. 2023, 23, 276.

Manuscript received: July 23, 2024 Accepted manuscript online: September 20, 2024 Version of record online: October 31, 2024